Research Square

Preprints are preliminary reports that have not undergone peer review.
They should not be considered conclusive, used to inform clinical practice,
or referenced by the media as validated information.

Neuroprotection by Ertugliflozin in Experimental Sepsis: Modulation of NF- κB/NLRP3-Associated Neuroinflammation and Oxidative Damage

Yasser J.H. Alyassery

Yasseralyassery@Alzahraa.edu.iq

Al-Zahraa University for Women

Research Article

Keywords: Ertugliflozin, sepsis-associated encephalopathy, cecal ligation and puncture, NLRP3 inflammasome, NF-κB, neuroinflammation, oxidative stress

Posted Date: November 23rd, 2026

DOI: https://doi.org/10.21203/rs.3.rs-11478421/v1

License: This work is licensed under a Creative Commons Attribution 4.0 International License.
Read Full License

Additional Declarations: No competing interests reported.

Neuroprotection by Ertugliflozin in Experimental Sepsis: Modulation of NF-κB/NLRP3-Associated Neuroinflammation and Oxidative Damage

Yasser J.H. Alyassery[1]
[1]College of Pharmacy, Al-Zahraa University for Women, Karbala, Iraq

First Author (corresponding)
Yasser J.H. Alyassery
College of Pharmacy, Al-Zahraa University for Women, Karbala, Iraq
https://orcid.org/0009-0002-7538-4478
Yasseralyassery@Alzahraa.edu.iq
yasserelyassery@gmail.com
+9647731973802

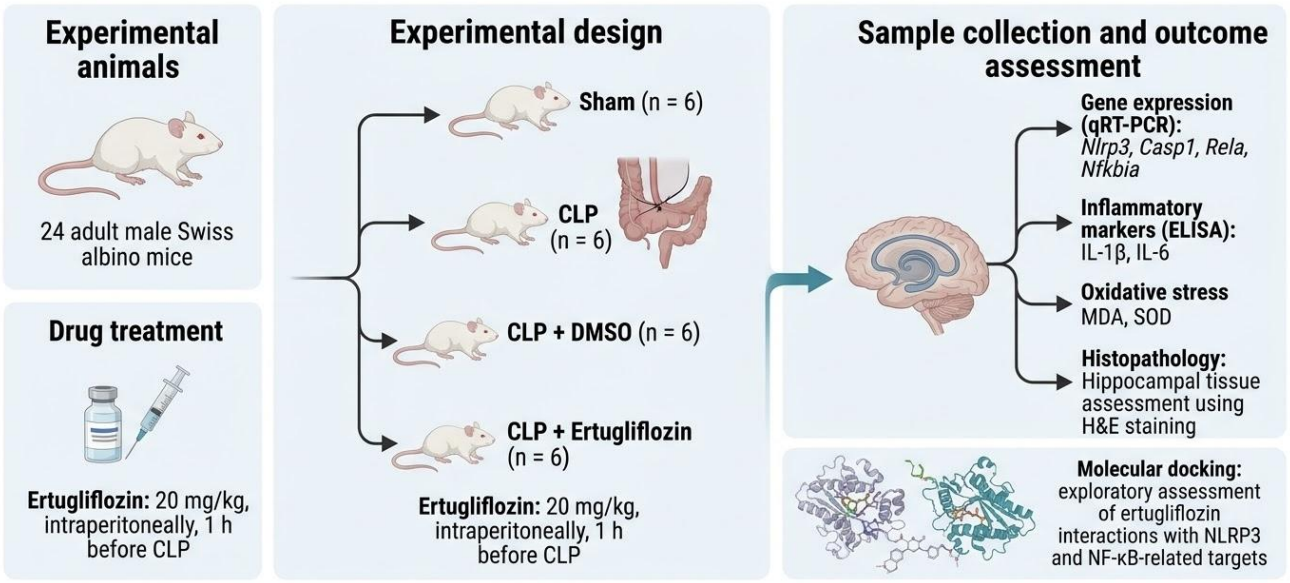
Neuroprotection by Ertugliflozin in Experimental Sepsis: Modulation of NF-κB/NLRP3-Associated Neuroinflammation and Oxidative Damage

Abstract

Sepsis-associated encephalopathy (SAE) is a serious complication of sepsis associated with persistent cognitive and functional impairment, with no specific pharmacological treatment currently available. This study investigated the neuroprotective effects of ertugliflozin, a sodium–glucose cotransporter 2 (SGLT2) inhibitor, in a mouse model of cecal ligation and puncture (CLP)-induced sepsis. Twenty-four adult male Swiss albino mice were randomly assigned to four groups (n = 6): sham, CLP, CLP plus vehicle (dimethyl sulfoxide), and CLP plus ertugliflozin (20 mg/kg, intraperitoneally), administered 1 h before CLP. Hippocampal expression of Nlrp3, Casp1, Rela, and Nfkbia was quantified using quantitative reverse-transcription polymerase chain reaction. Interleukin (IL)-1β, IL-6, malondialdehyde (MDA), and superoxide dismutase (SOD) were assessed using enzyme-linked immunosorbent assays. Histopathological injury was evaluated semiquantitatively, and molecular docking examined predicted ertugliflozin interactions with human NLRP3 and NF-κB. Compared with sham, CLP significantly increased Nlrp3, Casp1, and Rela expression while decreasing Nfkbia expression. These changes were accompanied by elevated IL-1β, IL-6, and MDA levels, reduced SOD activity, and increased histopathological injury. Ertugliflozin pretreatment significantly attenuated these molecular and biochemical alterations and reduced histopathological damage. Molecular docking predicted binding energies of −9.1 kcal/mol for NLRP3 and −7.6 kcal/mol for NF-κB. The predicted NLRP3 binding pose involved the NACHT domain and overlapped with the reported MCC950-binding pocket. Collectively, these findings suggest that ertugliflozin pretreatment mitigates CLP-associated hippocampal inflammation, oxidative stress, and tissue injury, potentially through modulation of NF-κB/NLRP3/caspase-1-associated signaling. Further studies are needed to establish its molecular mechanisms and therapeutic efficacy when administered after sepsis onset.

Keywords: Ertugliflozin; sepsis-associated encephalopathy; cecal ligation and puncture; NLRP3 inflammasome; NF-κB; neuroinflammation; oxidative stress.

Graphical Abstract:



Introduction

Sepsis is defined as life-threatening organ dysfunction caused by a dysregulated host response to infection (Jarczak, Kluge, and Nierhaus 2021). It remains a leading cause of death worldwide: the Global Burden of Disease Study estimated 48.9 million incident cases and 11.0 million sepsis-related deaths in 2017, accounting for almost one in five deaths globally (Via et al. 2026). Improvements in early resuscitation and antimicrobial therapy have increased short-term survival, but a growing number of survivors are left with lasting morbidity. Among the most disabling consequences is injury to the brain, which can appear early as sepsis-associated encephalopathy (SAE) and persist as long-term cognitive impairment (Zhou et al. 2024). In a landmark cohort, survivors of severe sepsis showed a substantial and sustained rise in moderate-to-severe cognitive impairment and functional disability compared with their pre-sepsis baseline (Basu et al. 2025). No specific pharmacological therapy for SAE exists, and management remains supportive (He et al. 2024).

The pathogenesis of SAE is multifactorial and involves blood–brain barrier disruption, microglial activation, mitochondrial dysfunction, and excessive generation of reactive oxygen species (Xiao et al. 2025). The hippocampus, which is central to learning and memory, is particularly vulnerable to these insults. Pro-inflammatory cytokines such as interleukin-1β (IL-1β) and interleukin-6 (IL-6) impair synaptic plasticity and neurogenesis when they are chronically elevated in this region (Imbriani et al. 2026). Oxidative stress both results from and amplifies this inflammatory milieu. Lipid peroxidation products such as malondialdehyde (MDA) accumulate, and endogenous antioxidant defences, including superoxide dismutase (SOD), are depleted (Lin et al. 2025).

Two interconnected signaling systems are thought to be at the core of this response. Nuclear factor kappa B (NF-κB) is a master transcriptional regulator of innate immunity; in resting cells it is held inactive in the cytoplasm by inhibitor of κB proteins, chiefly IκB-α, and its activation drives the expression of numerous pro-inflammatory genes (Piotr 2022). NF-κB activation has long been implicated in the pathological response to sepsis. It also provides the “priming” signal that induces transcription of NLRP3 and pro-IL-1β (Bauernfeind et al. 2010). The NOD-like receptor family pyrin domain-containing 3 (NLRP3) inflammasome is a multiprotein complex that, once assembled, activates caspase-1, which cleaves pro-IL-1β into its mature form and triggers gasdermin D-mediated pyroptosis (Chen et al. 2022). Aberrant NLRP3 activation in the brain has been shown to contribute to neuroinflammation and pathology in neurodegenerative disease,

making the NF-κB/NLRP3/caspase-1 axis an attractive therapeutic target in sepsis-induced brain injury (Id et al. 2020).

Sodium–glucose cotransporter 2 (SGLT2) inhibitors were developed as glucose-lowering drugs for type 2 diabetes, but large outcome trials revealed unexpected cardiovascular and renal benefits that exceed what glycaemic control alone would predict (Dabravolski et al. 2022). Ertugliflozin, the most recently approved member of the class, was shown to be non-inferior to placebo for major adverse cardiovascular events in the VERTIS CV trial (Liu et al. 2022). Mechanistic studies suggest that these benefits are partly mediated by anti-inflammatory and antioxidant effects(Fediuk et al. 2020; Hassan et al. 2025). In particular, SGLT2 inhibitors suppress NLRP3 inflammasome activation, an effect attributed to altered ketone metabolism and reduced insulin and glucose signalling, and empagliflozin and dapagliflozin attenuate NLRP3/ASC activation in metabolic and cardiac disease models (Quagliariello et al. 2021). SGLT2 inhibitors have also shown neuroprotective potential in preclinical models, including improved vascular integrity and cognition in a mouse model of Alzheimer's disease with diabetes (Han et al. 2025). Whether ertugliflozin protects the brain during sepsis, and whether it acts on the NF-κB/NLRP3 axis in the hippocampus, has not been examined.

The present study therefore investigated the effect of ertugliflozin pre-treatment on hippocampal injury in the cecal ligation and puncture (CLP) model, which closely reproduces the polymicrobial course of human sepsis. Accordingly, this study investigated the effects of ertugliflozin on hippocampal inflammatory signaling, oxidative stress, and histopathological alterations in a mouse model of sepsis. Specifically, we assessed the transcript levels of Nlrp3, Casp1, Rela (encoding NF-κB p65), and Nfkbia (encoding IκB-α), alongside hippocampal IL-1β and IL-6 levels, malondialdehyde (MDA) and superoxide dismutase (SOD) as indices of oxidative stress, and histopathological changes. Additionally, molecular docking was performed to explore the potential direct interactions of ertugliflozin with NLRP3 and NF-κB, providing complementary in silico insights into its possible molecular mechanisms of action.

Methods

Animal Preparation

A total of 24 adult albino Swiss mice, aged 8–12 weeks and weighing 25–35 g, were obtained from the animal husbandry facility of the Faculty of Science, University of Kufa, Iraq. The animals were housed in a dedicated room within the same facility under controlled environmental conditions,

with a 12-h light/12-h dark cycle, an ambient temperature of 24 ± 2 °C, and relative humidity of 60–65%. Standard laboratory chow and water were provided *ad libitum*. All experimental procedures were reviewed and approved by the Institutional Animal Care and Use Committee (IACUC) of the University of Kufa (approval number: 2111, 1/1/2025) and were conducted in accordance with the committee's applicable guidelines for the care and use of laboratory animals.

Study Design

Twenty-four adult male Swiss albino mice were randomly allocated into four experimental groups (n = 6 per group): sham, cecal ligation and puncture (CLP), CLP + dimethyl sulfoxide (DMSO), and CLP + ertugliflozin. The sham group underwent anesthesia and a midline laparotomy without cecal ligation or puncture. In the remaining groups, sepsis was induced using the CLP procedure (Schreyer et al. 2026). Briefly, under intraperitoneal anesthesia with ketamine (80 mg/kg) and xylazine (5 mg/kg) (Beecy et al. 2025)(Veilleux-lemieux et al. 2012), a 1.5-cm midline abdominal incision was made to expose the cecum. Approximately 75% of the cecal length was ligated just distal to the ileocecal valve using 5-0 surgical suture. The ligated cecum was then punctured twice using a 22-gauge needle, which was carefully withdrawn, followed by gentle compression of the cecum to extrude a small amount of fecal material through the puncture sites. The cecum was subsequently returned to the abdominal cavity, and the incision was closed using 6-0 silk sutures. Immediately after surgery, 1 mL of prewarmed sterile normal saline (37 °C) was administered intraperitoneally to compensate for fluid loss (Schreyer et al. 2026). The CLP + DMSO group received DMSO, the vehicle for ertugliflozin, via intraperitoneal injection 1 h before CLP induction, whereas the CLP + ertugliflozin group received ertugliflozin (20 mg/kg, intraperitoneally) at the same time point(Wang et al. 2026).

Preparation of Ertugliflozin

Ertugliflozin was dissolved in dimethyl sulfoxide (DMSO) at a concentration of 50 mg/mL (100 mg in 2 mL) and freshly prepared immediately before administration. The dose was adjusted according to the body weight of each animal and administered via intraperitoneal injection at 20 mg/kg(Wang et al. 2026).

Tissue Collection and Processing

The animals were deeply anesthetized with ketamine (80 mg/kg) and xylazine (5 mg/kg) before euthanasia(Beecy et al. 2025)(Veilleux-lemieux et al. 2012). The brains were rapidly excised, and the hippocampi were carefully dissected on an ice-cold surface to minimize postmortem tissue degradation. The dissected tissues were briefly rinsed with ice-cold phosphate-buffered saline (PBS), where appropriate, gently blotted to remove excess fluid, weighed, and allocated for subsequent biochemical and molecular analyses. For biochemical assays, designated hippocampal tissue samples were homogenized in an appropriate ice-cold homogenization buffer and centrifuged at 4 °C for 10 min. The resulting supernatants were collected and stored at −80 °C until analysis using enzyme-linked immunosorbent assay (ELISA). Separate hippocampal tissue samples designated for gene-expression analysis were immediately immersed in TRIzol reagent and stored at −80 °C until RNA extraction. Total RNA was subsequently extracted using TRIzol reagent according to the manufacturer's instructions.

Assessment of Oxidative Stress

The levels of malondialdehyde (MDA) and superoxide dismutase (SOD) in hippocampal tissue homogenates were quantified using commercially available ELISA kits (Sunlong Biotech Co., Ltd., Hangzhou, China), according to the manufacturer's instructions. MDA and SOD concentrations were measured using the MDA ELISA Kit (Cat. No. SL0475Ra) and SOD ELISA Kit (Cat. No. SL0664Ra), respectively. Increased MDA levels were interpreted as an indicator of enhanced lipid peroxidation and oxidative damage, whereas SOD levels were assessed to evaluate endogenous antioxidant defense(Bizoń et al. 2023; Gowda et al. 2022).

Assessment of Neuroinflammatory Cytokines

The concentrations of interleukin-6 (IL-6) and interleukin-1β (IL-1β) in hippocampal tissue homogenates were determined using commercially available ELISA kits (Sunlong Biotech Co., Ltd., Hangzhou, China), according to the manufacturer's instructions. IL-6 and IL-1β concentrations were measured using the IL-6 ELISA Kit (Cat. No. SL0411Ra) and IL-1β ELISA Kit (Cat. No. SL0402Ra), respectively. These proinflammatory cytokines were assessed to evaluate neuroinflammatory responses associated with CLP-induced sepsis and the potential anti-inflammatory effects of ertugliflozin.

RNA Extraction and Quantitative Real-Time PCR

Total RNA was extracted from hippocampal tissue samples using AccuZol™ RNA Extraction Reagent (Bioneer Corporation, Daejeon, Republic of Korea) according to the manufacturer's instructions. Briefly, tissue samples were homogenized in AccuZol™ reagent, followed by phase separation, RNA precipitation, washing, and dissolution of the purified RNA. The concentration and purity of the extracted RNA were assessed spectrophotometrically by measuring absorbance at 260 and 280 nm, respectively, and RNA purity was evaluated using the A260/A280 ratio. Equal amounts of RNA were subsequently reverse-transcribed into complementary DNA (cDNA) using a commercial reverse-transcription kit according to the manufacturer's instructions. Quantitative real-time polymerase chain reaction (qRT-PCR) was performed using SYBR Green chemistry to determine the relative mRNA expression levels of NOD-like receptor family pyrin domain-containing 3 (*Nlrp3*), nuclear factor kappa B (*Rela*, encoding the p65 subunit), nuclear factor kappa B inhibitor alpha (*Nfkbia*, encoding IκB-α), and caspase-1 (*Casp1*). Glyceraldehyde-3-phosphate dehydrogenase (*Gapdh*) was used as the housekeeping reference gene for normalization. The primer sequences used for amplification are presented in Table 1. The qRT-PCR reactions were performed using a SYBR Green-based master mix in a real-time PCR system according to the manufacturer's instructions. The amplification program consisted of an initial denaturation step followed by repeated cycles of denaturation, annealing, and extension. Melting-curve analysis was performed after amplification to assess the specificity of the PCR products. The cycle threshold (Ct) values of the target genes were normalized to the corresponding *Gapdh* Ct values to calculate ΔCt values. Relative mRNA expression was determined using the comparative $2^{-}\Delta\Delta Ct$ method, with the designated control group serving as the calibrator. ΔΔCt values were calculated by subtracting the mean ΔCt of the control group from the ΔCt of each experimental sample (Livak and Schmittgen 2001). Gene expression results were expressed as relative fold changes compared with the control group.

Table 1. Primer sequences used for quantitative real-time polymerase chain reaction (qRT-PCR).

Gene	Forward primer (5′–3′)	Reverse primer (5′–3′)
Nlrp3	ATTACCCGCCCGAGAAAGG	TCGCAGCAAAGATCCACACAG

Rela (p65)	CTTCCTCAGCCATGGTACCTCT	CAAGTCTTCATCAGCATCAAACTG
Nfkbia (IκB-α)	TGAAGGACGAGGAGTACGAGC	TTCGTGGATGATTGCCAAGTG
Casp1	AGGAATTCTGGAGCTTCAATCAG	TGGAAATGTGCCATCTTCTTT
Gapdh	AGGTCGGTGTGAACGGATTTG	TGTAGACCATGTAGTTGAGGTCA

Histopathological examination

Brain specimens were fixed in 10% formalin, subjected to dehydration using ascending concentrations of ethanol (60–100%), cleared with xylene, and embedded in paraffin wax. Sections of 5 μm thickness were cut horizontally, stained with hematoxylin and eosin (H&E), and evaluated histologically by a pathologist blinded to the treatment groups (Liaquat et al. 2019). Histopathological damage was graded on a 0–3 scale according to the severity of tissue alterations. Score 1 represented mild changes, including edema, neuronal pyknosis, eosinophilic infiltration, and/or shrunken, hyperchromatic eosinophilic neurons indicative of atrophy. Score 2 indicated moderate tissue damage, characterized by the presence of at least two hemorrhagic areas. Score 3 denoted severe histopathological injury, evidenced by clearly defined infarcted foci or localized areas of necrosis (La 2003; Shnaien, Mohammad, and Hassan 2023).

Molecular Docking and Interaction Analysis

The three-dimensional structure of ertugliflozin was retrieved from the PubChem database in SDF format, while the crystal structures of the human NLRP3 NACHT domain (PDB ID: 7ALV) and NF-κB (PDB ID: 1LE5) were obtained from the RCSB Protein Data Bank. Protein structures and the ligand were submitted to the CB-Dock2 server (https://cadd.labshare.cn/cb-dock2/), which integrates curvature-based cavity detection (CurPocket), AutoDock Vina-based docking, and homologous template fitting. The server automatically prepared the protein structures by removing non-protein components and adding hydrogen atoms and partial charges, identified potential binding cavities, and generated docking search boxes according to the detected cavity dimensions and ligand size. Blind molecular docking was performed, and the binding pose with the lowest

predicted binding energy (Vina score, kcal/mol) in the top-ranked cavity was selected for subsequent analysis, with more negative scores indicating more favorable predicted binding affinity. Protein–ligand interactions were subsequently examined using two- and three-dimensional visualizations. Two-dimensional interaction diagrams were generated using Schrödinger Maestro (Schrödinger LLC, New York, NY, USA), while three-dimensional binding poses were visualized using the CB-Dock2 viewer. Hydrogen bonds, hydrophobic contacts, and other predicted interactions were examined according to the visualization software's graphical conventions, and the resulting images were assembled into labeled composite figures.

Statistical Analysis

Statistical analyses were performed using GraphPad Prism version 9 (GraphPad Software, San Diego, CA, USA). Data are presented as mean ± standard deviation (SD) for continuous variables and as median and interquartile range (IQR) for histopathological damage scores. Differences among the four experimental groups were evaluated using one-way analysis of variance (ANOVA), followed by Tukey's multiple-comparisons test for pairwise comparisons. Homogeneity of variances was assessed using appropriate tests, including the Brown–Forsythe and Bartlett tests. Histopathological damage scores were analyzed using the Kruskal–Wallis test, followed by Dunn's multiple-comparisons test. All statistical tests were two-sided, and ($P < 0.05$) was considered statistically significant.

3. Results

Effect of ertugliflozin on NLRP3 inflammasome and NF-κB pathway gene expression

Sepsis induced by CLP produced a pronounced up-regulation of the central components of the NLRP3 inflammasome and NF-κB pathways in comparison with Sham animals, and pre-treatment with ertugliflozin markedly attenuated this response. Group means and ANOVA results for these genes are summarized in Table 2.

Table 2. Relative mRNA expression (fold change versus Sham) of NLRP3, caspase-1 and NF-κB (mean ± SD).

Gene	Sham	CLP	CLP + DMSO	CLP + Ertu	P value

NLRP3	1.08 ± 0.53	24.98 ± 11.00	27.41 ± 3.97	7.90 ± 2.57	0.0016
Caspase-1	1.05 ± 0.39	38.28 ± 17.55	35.44 ± 10.87	7.97 ± 3.33	0.0047
NF-κB	1.18 ± 0.67	44.89 ± 9.82	42.38 ± 9.37	11.90 ± 6.62	0.0002

NLRP3 gene expression

Compared with the Sham group, NLRP3 expression was significantly elevated in both the CLP group (adjusted P = 0.0053) and the CLP + DMSO group (adjusted P = 0.0029). No significant difference was observed between the CLP and CLP + DMSO groups (adjusted P = 0.9578), suggesting that DMSO administration did not significantly affect NLRP3 expression. Pre-treatment with ertugliflozin significantly attenuated NLRP3 upregulation compared with both the CLP group (adjusted P = 0.0334) and the CLP + DMSO group (adjusted P = 0.0169). Furthermore, NLRP3 expression in the CLP + Ertu group did not differ significantly from that in the Sham group (adjusted P = 0.5358), indicating that ertugliflozin attenuated the CLP-associated increase in NLRP3 expression (Figure 1A).

Caspase-1 gene expression

Compared with the Sham group, caspase-1 expression was significantly elevated in both the CLP group (adjusted P = 0.0104) and the CLP + DMSO group (adjusted P = 0.0160). No significant difference was observed between the CLP and CLP + DMSO groups (adjusted P = 0.9865), indicating that DMSO did not significantly influence caspase-1 expression. Ertugliflozin pre-treatment significantly reduced caspase-1 expression compared with both the CLP group (adjusted P = 0.0308) and the CLP + DMSO group (adjusted P = 0.0490). Furthermore, caspase-1 expression in the CLP + Ertu group did not differ significantly from that in the Sham group (adjusted P = 0.8479), suggesting that ertugliflozin attenuated the CLP-associated increase in caspase-1 expression (Figure 1B).

NF-κB gene expression

Compared with the Sham group, NF-κB expression was significantly elevated in both the CLP group (adjusted P = 0.0005) and the CLP + DMSO group (adjusted P = 0.0007). Ertugliflozin pre-treatment significantly attenuated NF-κB upregulation compared with both the CLP group (adjusted P = 0.0031) and the CLP + DMSO group (adjusted P = 0.0050). Furthermore, NF-κB expression in the CLP + Ertu group did not differ significantly from that in the Sham group

(adjusted P = 0.3664), suggesting that ertugliflozin mitigated the CLP-associated increase in NF-κB expression (Figure 1C).

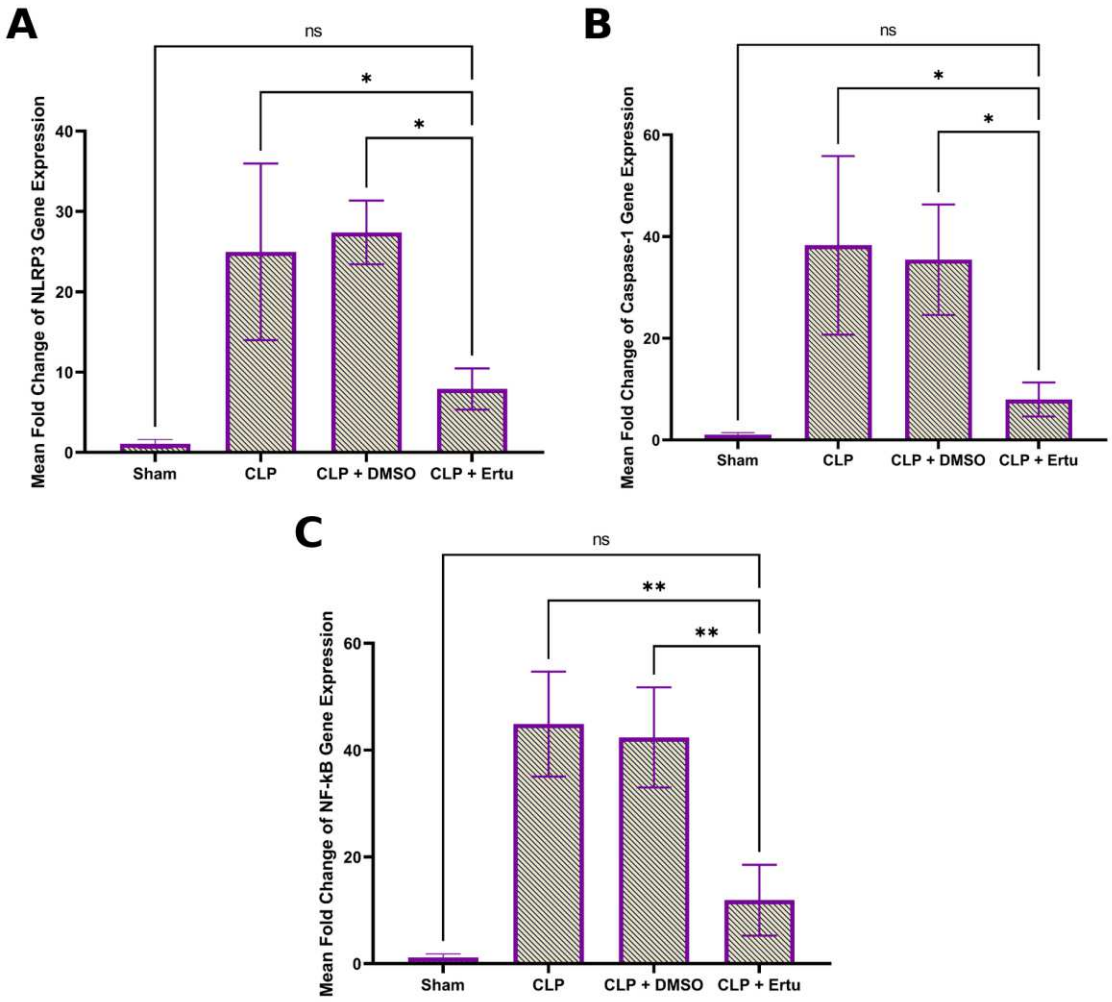


Figure 1. Effect of ertugliflozin pre-treatment on NLRP3 inflammasome and NF-κB gene expression in CLP-induced sepsis. Relative mRNA expression of (A) NLRP3, (B) caspase-1 and (C) NF-κB, shown as mean fold change versus Sham. Error bars represent SD. Brackets indicate Tukey's post hoc comparisons of the CLP + Ertu group with the other groups: *P < 0.05, **P < 0.01; ns, not significant. Differences of the CLP and CLP + DMSO groups versus Sham are reported in the text. CLP, cecal ligation and puncture; DMSO, dimethyl sulfoxide; Ertu, ertugliflozin.

IκB-α gene expression

Because IκB-α is an endogenous inhibitor of NF-κB, its transcript levels were analysed using ΔCt values, calculated as the target gene Ct minus the reference gene Ct, whereby higher ΔCt values

indicate lower gene expression. Compared with the Sham group, ΔCt values were significantly higher in both the CLP and CLP + DMSO groups (adjusted P = 0.0002 for both comparisons), with no significant difference between these groups (adjusted P = 0.9982), indicating substantial suppression of IκB-α expression (Figure 2A).

Ertugliflozin pre-treatment significantly reduced ΔCt values compared with both the CLP group (adjusted P = 0.0004) and the CLP + DMSO group (adjusted P = 0.0004). Furthermore, ΔCt values in the CLP + Ertu group did not differ significantly from those in the Sham group (adjusted P = 0.9184).

Consistent with these findings, fold-change analysis showed that IκB-α expression decreased markedly in both the CLP and CLP + DMSO groups relative to Sham, whereas ertugliflozin pre-treatment restored expression toward baseline levels (Figure 2B). Together with the observed changes in NF-κB expression, these findings suggest that ertugliflozin attenuated NF-κB pathway activation, at least partly by preserving IκB-α expression.

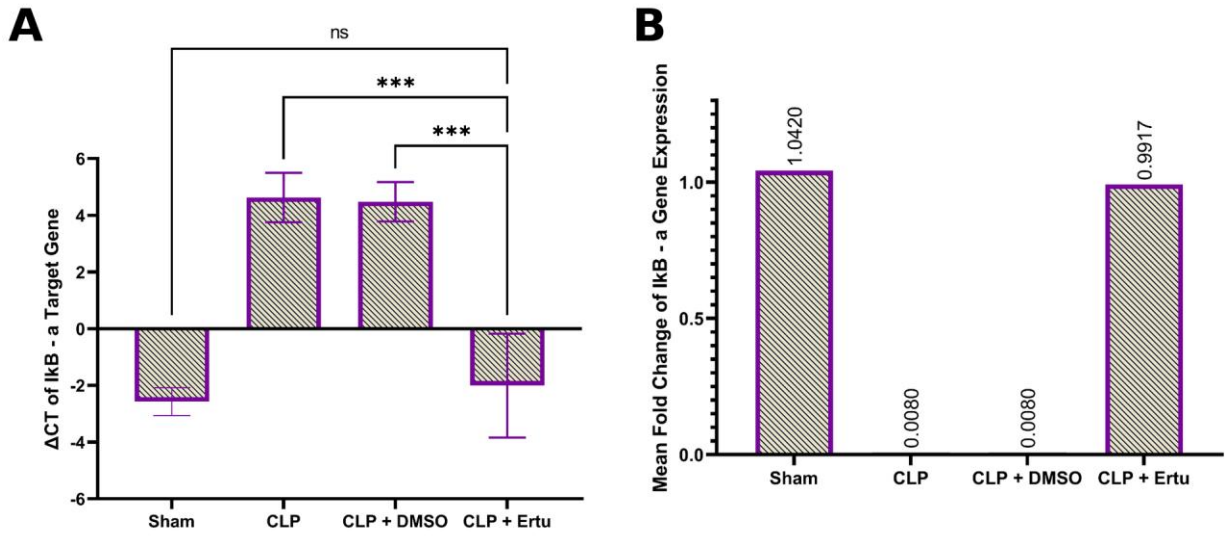


Figure 2. Effect of ertugliflozin pre-treatment on IκB-α gene expression in CLP-induced sepsis. (A) ΔCt values of IκB-α (mean ± SD); a higher ΔCt indicates lower expression. Brackets indicate Tukey's post hoc comparisons of the CLP + Ertu group with the other groups: ***P < 0.001; ns, not significant. (B) Mean fold change of IκB-α expression derived from the ΔCt values, with mean values printed above the bars; shown descriptively, without a separate statistical test.

Effect of ertugliflozin on pro-inflammatory cytokines

Sepsis significantly increased IL-1β and IL-6 levels compared with the Sham group (adjusted $P < 0.0001$ for all comparisons). Neither cytokine differed significantly between the CLP and CLP + DMSO groups (adjusted $P = 0.9818$ for IL-1β and $P = 0.6352$ for IL-6), indicating no significant effect of vehicle administration (Table 3).

Ertugliflozin pre-treatment significantly reduced IL-1β levels compared with both the CLP and CLP + DMSO groups (adjusted $P < 0.0001$ for both comparisons). However, IL-1β remained significantly higher than in the Sham group (adjusted $P = 0.0204$; Figure 3A).

Similarly, ertugliflozin significantly attenuated the sepsis-associated elevation in IL-6 compared with both the CLP and CLP + DMSO groups (adjusted $P < 0.0001$ for both comparisons). IL-6 levels in the CLP + Ertu group did not differ significantly from those in the Sham group (adjusted $P = 0.9529$; Figure 3B). These findings indicate that ertugliflozin markedly attenuated the systemic inflammatory response, with IL-6 returning to levels comparable to those of the Sham group, whereas IL-1β remained modestly elevated.

Table 3. Cytokine and oxidative stress markers (mean ± SD).

Marker	Sham	CLP	CLP + DMSO	CLP + Ertu	P value
IL-1β (pg/mL)	30.02 ± 6.39	117.7 ± 12.12	120.2 ± 17.64	51.48 ± 5.70	< 0.0001
IL-6 (pg/mL)	42.44 ± 11.97	102.8 ± 11.36	111.6 ± 14.59	46.23 ± 12.18	< 0.0001
MDA (ng/mL)	41.26 ± 8.60	115.9 ± 8.98	108.3 ± 12.78	52.23 ± 6.01	< 0.0001
SOD (pg/mL)	480.3 ± 41.91	132.5 ± 30.29	150.5 ± 26.23	280.5 ± 71.60	< 0.0001

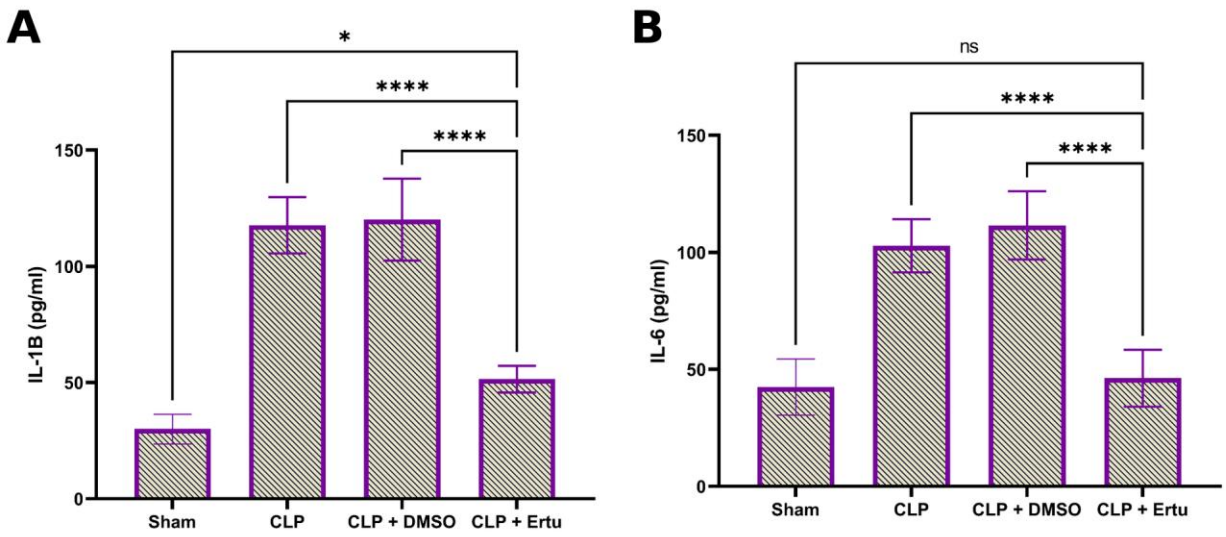


Figure 3. Effect of ertugliflozin pre-treatment on pro-inflammatory cytokines in CLP-induced sepsis. Concentrations of (A) IL-1β and (B) IL-6 (pg/mL; mean ± SD). Brackets indicate Tukey's post hoc comparisons of the CLP + Ertu group with the other groups: *P < 0.05, ****P < 0.0001; ns, not significant.

Effect of ertugliflozin on oxidative stress markers

Compared with the Sham group, MDA levels were significantly elevated in both the CLP and CLP + DMSO groups (adjusted P < 0.0001 for both comparisons). No significant difference was observed between the two septic control groups (adjusted P = 0.5136), indicating no significant effect of vehicle administration. Ertugliflozin pre-treatment significantly reduced MDA levels compared with both the CLP and CLP + DMSO groups (adjusted P < 0.0001 for both comparisons). Furthermore, MDA levels in the CLP + Ertu group did not differ significantly from those in the Sham group (adjusted P = 0.2144), suggesting that ertugliflozin effectively attenuated lipid peroxidation (Figure 4A).

SOD levels were significantly reduced in both the CLP and CLP + DMSO groups compared with Sham (adjusted P < 0.0001 for both comparisons), with no significant difference between the septic control groups (adjusted P = 0.9051). Ertugliflozin pre-treatment significantly increased SOD levels compared with both the CLP group (adjusted P = 0.0001) and the CLP + DMSO group

(adjusted P = 0.0005). However, SOD levels remained significantly lower than those in the Sham group (adjusted P < 0.0001), indicating partial restoration of antioxidant capacity (Figure 4B).

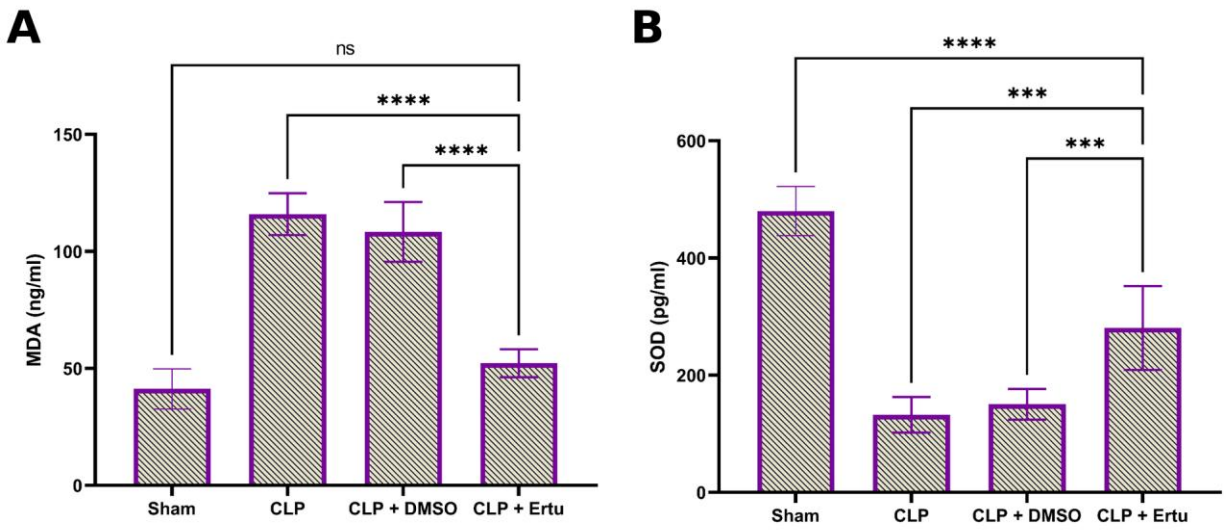


Figure 4. Effect of ertugliflozin pre-treatment on oxidative stress markers in CLP-induced sepsis. Levels of (A) malondialdehyde (MDA, ng/mL) and (B) superoxide dismutase (SOD, pg/mL) (mean ± SD). Brackets indicate Tukey's post hoc comparisons of the CLP + Ertu group with the other groups: ***P < 0.001, ****P < 0.0001; ns, not significant.

Effect of ertugliflozin on histopathological damage

Histopathological damage scores differed significantly among the experimental groups (Kruskal–Wallis H = 19.46, P = 0.0002). Compared with the Sham group, both the CLP and CLP + DMSO groups exhibited significantly greater tissue damage (Dunn's adjusted P = 0.0033 for both comparisons). No significant difference was observed between the two septic control groups (adjusted P > 0.9999), indicating no detectable effect of vehicle administration.

Ertugliflozin pre-treatment significantly reduced histopathological damage compared with both the CLP and CLP + DMSO groups (Dunn's adjusted P = 0.0432 for both comparisons). Furthermore, damage scores in the CLP + Ertu group did not differ significantly from those in the

Sham group (adjusted P > 0.9999), suggesting that ertugliflozin substantially attenuated sepsis-associated tissue injury (Figure 5; Table 4).

Table 4. Histopathological damage scores.

Group	Median	25th percentile	75th percentile	Mean rank
Sham	0	0	0	5.0
CLP	2.5	2	3	18.5
CLP + DMSO	2.5	2	3	18.5
CLP + Ertu	0.5	0	1	8.0

Kruskal-Wallis test, H = 19.46, P = 0.0002; Dunn's multiple comparisons test.

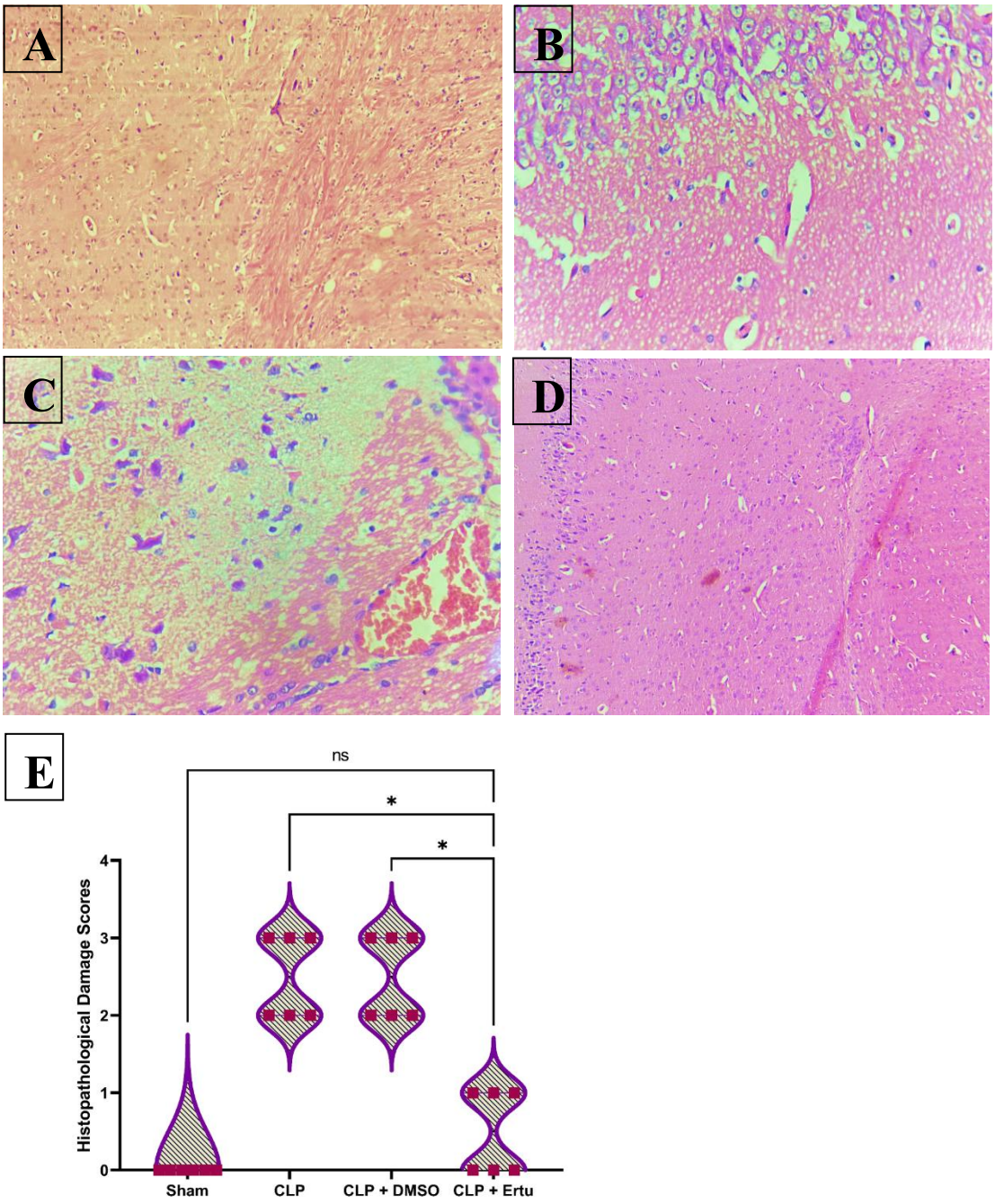


Figure 5. Representive histopathological photomicrographs and illustration of the effect of ertugliflozin pre-treatment on histopathological damage scores in CLP-induced sepsis. Violin plots with individual data points (n = 6 per group). Brackets indicate Dunn's post hoc comparisons of the CLP + Ertu group with the other groups: *P < 0.05; ns, not significant.

In silico molecular docking of ertugliflozin with NLRP3 and NF-kB

To explore whether ertugliflozin could interact directly with proteins that govern the inflammatory and oxidative pathways modulated in vivo, blind molecular docking was performed against the human NLRP3 NACHT domain (PDB ID: 7ALV) and NF-kB (PDB ID: 1LE5). The three-dimensional structure of ertugliflozin was retrieved from PubChem and docked using CB-Dock2, which combines curvature-based cavity detection with AutoDock Vina(Yang et al. 2022)(Olson 2011)(Eberhardt et al. 2023). The pose with the lowest predicted binding free energy (Vina score) in the top-ranked cavity was analysed, with more negative scores indicating stronger predicted affinity. Docking scores and the interactions identified are summarised in Table 4, and the predicted binding modes are shown in Figure 6.

Predicted binding affinity

Ertugliflozin docked favourably into both targets. The predicted binding affinity was −9.1 kcal/mol for NLRP3 and −7.6 kcal/mol for NF-kB, indicating a stronger predicted interaction with NLRP3 (a difference of 1.5 kcal/mol). Both scores lie within the range generally regarded as indicative of stable ligand binding in Vina-based screening (≤ −7.0 kcal/mol).

Interaction profile with NLRP3

The two-dimensional interaction diagram (Figure 6A) showed that ertugliflozin was accommodated in a pocket lined predominantly by hydrophobic residues. The hydroxymethyl group of the sugar-like bicyclic moiety formed a hydrogen bond with the side chain of Gln624, whereas the chlorophenyl and ethoxybenzyl rings were surrounded by Ala227, Phe410, Ile411, Pro352, Val353, Ile574, Phe575, Tyr632 and Met661, consistent with hydrophobic and van der Waals contacts stabilising the aglycone portion of the molecule. Polar residues (Ser626, Thr439 and Thr659) and charged residues (Arg351, Arg578 and Glu629) were located at the periphery of

the ligand and probably contribute electrostatic and polar stabilisation. The three-dimensional view (Figure 6B) confirmed this arrangement and additionally displayed short polar contacts around the hydroxyl groups of the ligand, hydrophobic contacts around the aromatic rings, and an electrostatic contact near Phe575 and Arg578.

Notably, several of the residues contacted by ertugliflozin (Arg351, Ala227, Ile411, Phe575, Arg578, Thr439 and Met661) have been described as lining the NACHT-domain pocket occupied by the inhibitor MCC950 in the 7ALV crystal structure (Dekker et al., 2021), suggesting that ertugliflozin may engage a pharmacologically relevant site.

Interaction profile with NF-kB

In the NF-kB complex (Figure 6C), ertugliflozin was stabilised by a hydrogen bond between its hydroxymethyl group and Asn186 (chain A) and by a π–cation interaction between the chlorophenyl ring and Arg305 (chain B). Hydrophobic contacts were limited to Ala192 (chain A) and Val303 (chain B), whereas the ligand was surrounded by polar residues (Asn186, Gln306 and Thr301) and a cluster of charged residues (Arg33, Arg187, Lys218, Lys275, Arg305 and Asp217). The three-dimensional pose (Figure 6D) showed multiple polar contacts towards the sugar-like ring and electrostatic contacts in the vicinity of Asp217, Lys218 and Arg305. The smaller hydrophobic contact area and the dependence on polar and charged contacts are in line with the weaker docking score relative to NLRP3.

Overall, binding to NLRP3 was driven mainly by hydrophobic contacts supplemented by one hydrogen bond, whereas binding to NF-kB relied on a hydrogen bond, a π–cation interaction and electrostatic contacts with charged residues (Table 5). These findings are predictive and hypothesis-generating; they indicate plausible direct engagement of both targets by ertugliflozin but do not, by themselves, establish binding or functional modulation.

Table 5. Docking scores and protein–ligand interactions of ertugliflozin with NLRP3 and NF-kB.

Parameter	NLRP3 (PDB 7ALV)	NF-kB (PDB 1LE5)
Vina score (kcal/mol)	−9.1	−7.6
Hydrogen bond	Gln624 (ligand hydroxymethyl OH → side chain)	Asn186, chain A (ligand hydroxymethyl OH → side chain)
π–cation interaction	None detected	Arg305, chain B ↔ chlorophenyl ring
Hydrophobic / van der Waals contacts	Ala227, Phe410, Ile411, Pro352, Val353, Ile574, Phe575, Tyr632, Met661	Ala192 (A), Val303 (B)
Polar residues in contact	Gln624, Ser626, Thr439, Thr659	Asn186 (A), Gln306 (B), Thr301 (B)
Charged residues in contact	Positive: Arg351, Arg578; negative: Glu629	Positive: Arg33, Arg187, Lys218 (A), Arg305, Lys275 (B); negative: Asp217 (A)

Residues are as displayed in the Maestro two-dimensional interaction diagrams; (A) and (B) denote protein chains of NF-kB . Vina score: more negative values indicate stronger predicted binding.

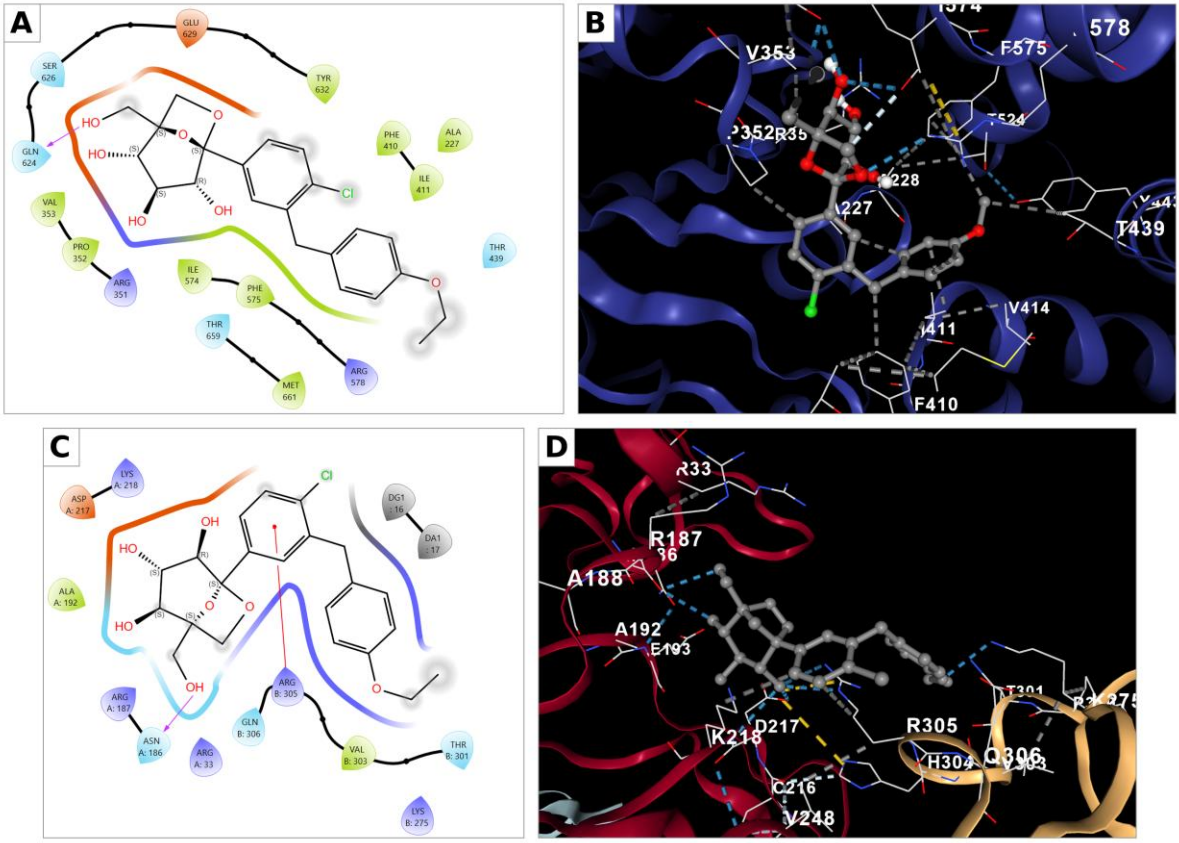


Figure 6. Predicted binding modes of ertugliflozin with NLRP3 and NF-kB. (A) Two-dimensional ligand interaction diagram and (B) three-dimensional view of ertugliflozin docked into NLRP3 (PDB 7ALV; Vina score −9.1 kcal/mol). (C) Two-dimensional interaction diagram and (D) three-dimensional view of ertugliflozin docked into NF-kB (PDB 1LE5; Vina score −7.6 kcal/mol). In the 2D panels (Maestro), purple

arrows indicate hydrogen bonds and the red line indicates a π–cation interaction; residue colours denote hydrophobic (green), polar (cyan), negatively charged (red), positively charged (purple) and other (grey) residues. In the 3D panels (CB-Dock2), blue dashed lines indicate hydrogen bonds, grey dashed lines hydrophobic contacts, and yellow dashed lines electrostatic or π-type contacts. Ertugliflozin is shown as ball-and-stick.

Discussion

This study shows that a single intraperitoneal dose of ertugliflozin given before CLP markedly limited hippocampal inflammation, oxidative stress and tissue damage in septic mice. CLP produced a large increase in *Nlrp3*, *Casp1* and *Rela* transcripts, a profound loss of *Nfkbia* transcript, roughly four-fold and two-fold increases in IL-1β and IL-6, a nearly three-fold increase in MDA, and a 72% fall in SOD. Ertugliflozin reduced *Nlrp3*, *Casp1* and *Rela* expression relative to untreated CLP animals, restored *Nfkbia* to the sham level, lowered IL-1β, IL-6 and MDA, partially preserved SOD, and reduced histopathological scores. The CLP and CLP + DMSO groups did not differ on any endpoint, so the vehicle cannot account for the protection. Docking predicted favorable binding of ertugliflozin to NLRP3 (−9.1 kcal/mol) and, less strongly, to NF-κB (−7.6 kcal/mol).

The coordinated rise of *Rela*, *Nlrp3* and *Casp1* after CLP is consistent with the two-step model of inflammasome activation, in which NF-κB-dependent priming increases the abundance of NLRP3 and pro-IL-1β before a second signal drives assembly of the complex (Bauernfeind et al. 2010). Ertugliflozin attenuated every component of this axis, and its effect on IL-1β, the principal product of caspase-1, matches the transcriptional findings. The simplest interpretation is that ertugliflozin reduced both priming and downstream inflammasome output. This agrees with earlier reports that SGLT2 inhibitors dampen NLRP3 signalling in macrophages and in cardiac and metabolic tissue (Kim et al. 2020). To our knowledge, the present data extend this observation to the septic hippocampus and to ertugliflozin specifically.

Because *Nfkbia* is itself an NF-κB target gene that forms part of a negative feedback loop, a fall in its mRNA during strong NF-κB induction is unexpected(Biswas and Bagchi 2016). Hippocampal IL-1β and IL-6 were strongly elevated by CLP (Peixin *et al.*, 2017) and substantially reduced by

ertugliflozin. The greater residual IL-1β is of interest because IL-1β requires caspase-1 cleavage, and caspase-1 transcript, although lowered, was not measured at the activity level. Both cytokines are known to impair hippocampal synaptic plasticity and neurogenesis, so their reduction is relevant to the long-term cognitive sequelae documented in sepsis survivors.

Sepsis is accompanied by mitochondrial dysfunction and overproduction of reactive oxygen species that overwhelm endogenous defenses (Kim et al. 2026). The marked rise in MDA and the depletion of SOD in untreated septic mice reflect this imbalance. Ertugliflozin returned MDA to values statistically indistinguishable from sham but restored SOD only partially, indicating that its effect on lipid peroxidation was greater than its effect on antioxidant enzyme preservation. Reactive oxygen species and NLRP3 are mutually reinforcing, as oxidative stress is a recognized trigger of inflammasome assembly while inflammasome-driven inflammation increases further oxidant generation. It is therefore plausible that the antioxidant and anti-inflammatory effects of ertugliflozin are coupled rather than independent. Earlier work on empagliflozin has linked SGLT2 inhibition to AMPK activation and reduced inflammation and energy depletion (Chen et al. 2024), which could contribute to the redox effects seen here, although we did not investigate these pathways.

Untreated septic animals showed marked tissue injury, whereas ertugliflozin-treated animals had scores that did not differ from sham. This morphological protection parallels the molecular findings and suggests that attenuation of inflammation and oxidative stress translated into preservation of tissue structure. Because histological scoring in small groups is semi-quantitative and rank-based, these findings should be regarded as supportive rather than definitive.

The docking analysis was intended to generate hypotheses about direct target engagement. Ertugliflozin was predicted to bind NLRP3 with higher affinity (−9.1 kcal/mol) than NF-κB (−7.6 kcal/mol). Several contacted NLRP3 residues (Arg351, Ala227, Ile411, Phe575, Arg578, Thr439 and Met661) coincide with the NACHT-domain pocket occupied by the inhibitor MCC950 in the 7ALV structure. MCC950 is known to block the ATP-hydrolysis motif of the NACHT domain and thereby lock NLRP3 in an inactive state. Overlap with this pocket raises the possibility that ertugliflozin could directly interfere with NLRP3 activation, in addition to acting through the metabolic and signaling mechanisms described above. Docking scores nevertheless depend

strongly on the scoring function and search protocol, they do not account fully for protein flexibility or solvation, and they correlate imperfectly with experimental affinity. The mechanism by which a peripherally administered SGLT2 inhibitor limits hippocampal injury is not established by our data. Several non-exclusive explanations are possible. First, SGLT2 expression has been reported in some brain regions, and SGLT2 inhibitors have been shown to act on central neurons, but neuronal expression appears to be low, so a direct central action is uncertain. Second, ertugliflozin may reduce systemic inflammation and cytokine release, thereby limiting blood–brain barrier disruption and neuroinflammatory signalling. Third, SGLT2 inhibition raises circulating ketones, notably β-hydroxybutyrate, which directly inhibits NLRP3. Fourth, the in-silico findings raise the possibility of direct interaction with inflammasome components.

Limitations

First, ertugliflozin was administered as a single prophylactic dose 1 hour prior to CLP induction, meaning its translational relevance to septic patients who present after clinical onset needs to be established in post-insult therapeutic models. Second, a single high dose of 20 mg/kg intraperitoneally was utilized without establishing a dose–response relationship or evaluating clinically equivalent exposure levels. Third, molecular evaluation was restricted to mRNA expression analysis without assessing protein levels, phosphorylated p65, cleaved caspase-1, gasdermin D, or cell-type specific localization. Finally, docking results represent computational predictions that require experimental validation (e.g., surface plasmon resonance or direct enzymatic assays) to confirm direct target engagement.

Conclusions and future directions

Pre-treatment with ertugliflozin attenuated hippocampal NF-κB/NLRP3/caspase-1 pathway gene expression, reduced IL-1β and IL-6, limited lipid peroxidation, partially preserved SOD, and reduced histopathological injury in a mouse model of CLP-induced sepsis. Docking suggested that ertugliflozin can occupy the MCC950-binding region of NLRP3. Together, these findings identify ertugliflozin as a candidate for repurposing against sepsis-associated brain injury. Future studies should test post-insult dosing, include dose–response and drug-only controls, validate pathway changes at the protein level and with NLRP3 or caspase-1 inhibitors and knockout mice, assess behavioural and survival outcomes, and experimentally verify direct binding to NLRP3.

Author Contributions

Yasser J. H. Alyassery: Conceptualization, Methodology, Investigation, Data curation, Formal analysis, Visualization, Writing – original draft, Writing – review and editing, and Project administration. The author reviewed and approved the final version of the manuscript and accepts responsibility for its content.

Funding

This research received no specific grant from any funding agency in the public, commercial, or not-for-profit sectors.

Declaration of Competing Interest

The author declares that there are no known competing financial interests or personal relationships that could have appeared to influence the work reported in this paper.

Acknowledgments

The author gratefully acknowledges Al-Zahraa University for Women, Karbala, Iraq, for its institutional affiliation and academic support, and the University of Kufa, Iraq, for facilitating access to the animal research facilities and supporting the experimental procedures.

References

Basu, Sanjukta, Ziyan J. Wei, Atara Laor, Liga Bennetts, and Nina Ahmad. 2025. "Health - Related Quality of Life Among Patients Who Have Survived an Episode of Sepsis in the United States : A Systematic Review." *Infectious Diseases and Therapy* 14(2):385–400. doi: 10.1007/s40121-024-01106-x.

Bauernfeind, Franz, Gabor Horvath, Andrea Stutz, Emad S. Alnemri, David Speert, Teresa Fernandes-alnemri, Jianghong Wu, G. Brian, Katherine A. Fitzgerald, Veit Hornung, and Eicke Latz. 2010. "NF-KB Activating Pattern Recognition and Cytokine Receptors License NLRP3 Inflammasome Activation by Regulating NLRP3 Expression." 183(2):787–91. doi: 10.4049/jimmunol.0901363.NF-kB.

Beecy, Sidney, Desiree Meuse, Nicole Kizielewicz, Corinna Beale, and Denise Molk. 2025. "Optimization of Ketamine / Xylazine Anesthesia in Geriatric Mice." 64(4). doi: 10.30802/AALAS-JAALAS-25-010.

Biswas, Ria, and Angshuman Bagchi. 2016. "NFkB Pathway and Inhibition: An Overview." *Computational Molecular Biology* 6(1):1–20. doi: 10.5376/cmb.2016.06.0001.

Bizoń, Anna, Justyna Chojdak-Łukasiewicz, Sławomir Budrewicz, Anna Pokryszko-Dragan, and Agnieszka Piwowar. 2023. "Exploring the Relationship between Antioxidant Enzymes, Oxidative Stress Markers, and Clinical Profile in Relapsing–Remitting Multiple Sclerosis." *Antioxidants* 12(8). doi: 10.3390/antiox12081638.

Chen, Chih-chao Yang Kuan-hung, Ya Yue, Ben-chung Cheng Tsuen-wei Hsu, and John Y. Chiang. 2024. "SGLT2 Inhibitor Downregulated Oxidative Stress via Activating AMPK Pathway for Cardiorenal (CR) Protection in CR Syndrome Rodent Fed with High Protein Diet." 803–23.

Chen, Weiwei, Xue Teng, Hongmei Ding, Zhiyuan Xie, Ping Cheng, Zhihan Liu, Tao Feng, Xia Zhang, Wenjuan Huang, and Deqin Geng. 2022. "Nrf2 Protects against Cerebral Ischemia-Reperfusion Injury by Suppressing Programmed Necrosis and Inflammatory Signaling Pathways." *Annals of Translational Medicine* 10(6):285–285. doi: 10.21037/atm-22-604.

Dabravolski, Siarhei A., Alexander D. Zhuravlev, Andrey G. Kartuesov, Evgeny E. Borisov, Vasily N. Sukhorukov, and Alexander N. Orekhov. 2022. "Mitochondria-Mediated Cardiovascular Benefits of Sodium-Glucose Co-Transporter 2 Inhibitors."

Eberhardt, Jerome, Diogo Santos-martins, Andreas F. Tillack, and Stefano Forli. 2023. "AutoDock Vina 1.2.0: New Docking Methods, Expanded Force Field, and Python Bindings." 61(8):3891–98. doi: 10.1021/acs.jcim.1c00203.AutoDock.

Fediuk, Daryl J., Gianluca Nucci, Vikas Kumar Dawra, David L. Cutler, Neeta B. Amin, Steven G. Terra, Rebecca A. Boyd, Rajesh Krishna, and Vaishali Sahasrabudhe. 2020. "Overview of the Clinical Pharmacology of Ertugliflozin, a Novel Sodium-Glucose Cotransporter 2 (SGLT2) Inhibitor." *Clinical Pharmacokinetics* 59(8):949–65. doi: 10.1007/s40262-020-00875-1.

Gowda, B. Rudresh, N. Prakash, C. R. Santhosh, B. H. Pavithra, Rashmi Rajashekaraiah, M. L.

Sathyanarayana, Suguna Rao, Prashantkumar Waghe, K. R. Anja. Kumar, G. R. Shivaprasad, and Y. Muralidhar. 2022. “Effect of Telmisartan on Arsenic-Induced (Sub-Chronic) Perturbations in Redox Homeostasis, Pro-Inflammatory Cascade and Aortic Dysfunction in Wistar Rats.” *Biological Trace Element Research* 200(4):1776–90. doi: 10.1007/s12011-021-02804-0.

Han, Jihui, Jaehoon Song, Eun Sun, Jung Ji, Won Choi, Hye Young, and Ji Inhee. 2025. “SGLT2 Inhibition by Enavogliflozin Significantly Reduces Aβ Pathology and Restores Cognitive Function via Upregulation of Microglial AMPK Signaling in 5XFAD Mouse Model of Alzheimer ’ s Disease.” doi: 10.1111/acel.70101.

Hassan, Nourhan Hussien, Gehan M. Kamel, Hany M. Fayed, and Reda M. S. Korany. 2025. “Ertugliflozin , a SGLT-2 Inhibitor , Guards Against Thioacetamide-Induced Liver Fibrosis : The Nrf2 / HO-1 and TLR4 / TGF- B1 Pathways.” 10(3):34–47.

He, Rong-rong, Guo-li Yue, Mei-ling Dong, Jia-qi Wang, and Chen Cheng. 2024. “Sepsis Biomarkers : Advancements and Clinical Applications — A Narrative Review.”

Id, Denise C. Cornelius, Olivia K. Travis, Robert W. Tramel Id, Marivee Borges-, Cedar H. Baik, Mallory Greer, Chelsea A. Giachelli, and Geilda A. Tardo. 2020. “NLRP3 Inflammasome Inhibition Attenuates Sepsis-Induced Platelet Activation and Prevents Multi-Organ Injury in Cecal-Ligation Puncture.” 1–15. doi: 10.1371/journal.pone.0234039.

Imbriani, Paola, Clara D. Ambra, Roberta De Mori, Marta Ionta, Alessandro Renna, and Paola Bonsi. 2026. “Dysregulation of Immune Mediators and Synaptic Plasticity in Central Nervous System Disorders.”

Jarczak, Dominik, Stefan Kluge, and Axel Nierhaus. 2021. “Sepsis — Pathophysiology and Therapeutic Concepts.” 8(May):1–22. doi: 10.3389/fmed.2021.628302.

Kim, Minsoo, Phyu Phyu Khin, Hyeran Jung, Chang Woo Chae, and Byeong Hwa Jeon. 2026. “Mitochondrial Immunometabolism in Sepsis : From Oxidative Stress and MtDAMP Signaling to Biomarker-Guided Therapy.”

Kim, So Ra, Sang-guk Lee, Soo Hyun Kim, Jin Hee Kim, Eunhye Choi, Wonhee Cho, John Hoon Rim, Inhwa Hwang, Chan Joo Lee, Minyoung Lee, Chang-myung Oh, Justin Y. Jeon, Heon Yung Gee, Jeong-ho Kim, Byung-wan Lee, Eun Seok Kang, and Bong-soo Cha. 2020.

"SGLT2 Inhibition Modulates NLRP3 Inflammasome Activity via Ketones and Insulin in Diabetes with Cardiovascular Disease." *Nature Communications* 1–11. doi: 10.1038/s41467-020-15983-6.

La, Poke. 2003. *Predictors of Brain Injury after Experimental Hypothermic Circulatory Arrest*.

Liaquat, Laraib, Sadia Sadir, Zehra Batool, Saiqa Tabassum, Sidrah Shahzad, Asia Afzal, and Saida Haider. 2019. *Acute Aluminum Chloride Toxicity Revisited: Study on DNA Damage and Histopathological, Biochemical and Neurochemical Alterations in Rat Brain*. Vol. 217. Elsevier Inc.

Lin, Yijuan, Ahmad Alhaskawi, Lin Chen, Safwat Adel, and Abdo Moqbel. 2025. "Recent Advances in Understanding Oxidative Stress in Sepsis : Pathogenic Roles and Antioxidant Therapeutic Prospects - a Narrative Review." (November):1–21. doi: 10.3389/fphar.2025.1695992.

Liu, Li, Fang Hong Shi, Hua Xu, Yue Wu, Zhi Chun Gu, and Hou Wen Lin. 2022. "Efficacy and Safety of Ertugliflozin in Type 2 Diabetes: A Systematic Review and Meta-Analysis." *Frontiers in Pharmacology* 12(January):1–11. doi: 10.3389/fphar.2021.752440.

Livak, Kenneth J., and Thomas D. Schmittgen. 2001. "Analysis of Relative Gene Expression Data Using Real-Time Quantitative PCR and the 2-ΔΔCT Method." *Methods* 25(4):402–8. doi: 10.1006/meth.2001.1262.

Olson, Oleg Trott and Arthur J. 2011. "AutoDock Vina: Improving the Speed and Accuracy of Docking with a New Scoring Function, Efficient Optimization and Multithreading." 31(2):455–61. doi: 10.1002/jcc.21334.AutoDock.

Peixin huang1 Mark W lee Jr2 Keivan sadrerafi2 Daniel P heruth1 li Q Zhang1 Dev Maulik3, 4 shui Qing Ye1, 4 1. 2017. "MC-PPEA as a New and More Potent Inhibitor of CLP-Induced Sepsis and Pulmonary Inflammation than FK866." 629–41.

Piotr, B. 2022. "The Role of Nuclear Factor Kappa B (NF- κ B) in the Immune Response against Parasites." 1–24.

Quagliariello, Vincenzo, Michelino De Laurentiis, Domenica Rea, Antonio Barbieri, Maria Gaia Monti, Andreina Carbone, Andrea Paccone, Lucia Altucci, Mariarosaria Conte, Maria Laura Canale, Gerardo Botti, and Nicola Maurea. 2021. "The SGLT-2 Inhibitor Empagliflozin

Improves Myocardial Strain, Reduces Cardiac Fibrosis and pro-Inflammatory Cytokines in Non-Diabetic Mice Treated with Doxorubicin." *Cardiovascular Diabetology* 20(1):1–20. doi: 10.1186/s12933-021-01346-y.

Schreyer, Korbinian Felix, Julia Stettmer, Li Cheng Wu, Markus Ballmann, Johannes Krell, Gerhard Schneider, and Martin Schlegel. 2026. "Experimental Robustness and Reproducibility of the Murine Cecal Ligation and Puncture Sepsis Model." 0.

Shnaien, A. A., A. R. Mohammad, and E. S. Hassan. 2023. "Neuroprotective Effects of Semaglutide in Endotoxemia Mouse Model." *Iranian Journal of War and Public Health* 15(2):199–205. doi: 10.58209/ijwph.15.2.199.

Veilleux-lemieux, Daphnée, Francis Beaudry, Pierre Hélie, and Pascal Vachon. 2012. "Effects of Endotoxemia on the Pharmacodynamics and Pharmacokinetics of Ketamine and Xylazine Anesthesia in Sprague – Dawley Rats." 99–109.

Via, Luigi La, Salvatore Ferlito, Maria Stella, Di Modica, Andrea Marino, Giuseppe Nunnari, Bruno Cacopardo, Jerome Rene Lechien, Mario Lentini, Salvatore Lavalle, Giancarlo Carmelo Botto, Paolo Buscema, Loris Gruppuso, and Antonino Maniaci. 2026. "The Global Impact of Sepsis : Epidemiology , Recognition , Management , and Health System Challenges." 1–27.

Wang, Xiaona, Zhengqin Zhao, Limin Sun, Chao Gao, Li Wang, Daoqi Mei, Chanjuan Hao, Shuai Zhao, Xingxue Yan, Jing Liu, Lei Liu, Bin Guo, and Yaodong Zhang. 2026. "BRAIN COMMUNICATIONS Ertugliflozin Improves Animal Behaviours Associated with Oxidative Stress and Inflammation in a BTBR T + Itpr3tf / J Mouse Model of Autism." *Brain Communications* 8(2):1–14. doi: 10.1093/braincomms/fcag083.

Xiao, Dan, Xiao Wang, Wanting Liang, Yunshu Yang, Yuting Du, Chunmao Liu, Feiyang Xu, and Yang Yang. 2025. "Convergence of Sepsis-Associated Encephalopathy Pathogenesis onto Microglia."

Yang, Xiaocong, Jianhong Gan, Shuang Chen, and Zhi-xiong Xiao. 2022. "CB-Dock2 : Improved Protein – Ligand Blind Docking by Integrating Cavity Detection , Docking and Homologous." 50(May):159–64.

Zhou, Yue, Lu Bai, Wenjing Tang, Weiying Yang, and Lichao Sun. 2024. "Heliyon Research

Progress in the Pathogenesis of Sepsis-Associated Encephalopathy." *Heliyon* 10(12):e33458. doi: 10.1016/j.heliyon.2024.e33458.